Rotor Position Estimation of PMSM in Low Speed Region and Standstill Using Zero Voltage Vector Injection

Gaolin Wang, *Member, IEEE*, Junyao Kuang, Nannan Zhao, Guoqiang Zhang, and Dianguo Xu, *Fellow, IEEE*

***Abstract*—High frequency signal injection methods have been widely used in sensorless control of permanent magnet synchronous motor (PMSM) drives. However, the acoustic noise and torque ripples caused by the injected high frequency signal limit the application of the methods. To avoid these drawbacks, this paper proposes a position estimation method that combines derivative calculations of current and zero voltage vector (ZVV) injection, which is especially effective for zero- and low-speed operation of sensorless PMSM drives. This investigation mainly focuses on the extraction of rotor position from ZVV period and the improvements of the accuracy of estimated position. The PMSM equation is developed in the stationary frame when ZVV is applied. The proposed d-axis current allocation scheme ensures the application of the proposed method from no load to rated load. A modified SVPWM control strategy and a ZVV extension scheme are employed to improve the accuracy of estimated position, which also makes the method more realizable. Further, a novel current sampling method that selects two suitable phase currents for derivative calculation according to the voltage sector location is proposed, which can help reduce current derivative ripples and decrease position estimation errors. Finally, the effectiveness of the proposed position estimation strategy is verified on a 1.0 kW interior PMSM (IPMSM) drive platform.**

***Index Terms*—Acoustic noise reduction, current derivatives calculation, permanent magnet synchronous motor (PMSM), rotor position estimation, zero and low speeds, zero voltage vector injection.**

I. Introduction

In recent years, permanent magnet synchronous motor (PMSM) has been widely employed in home appliances and industrial applications. These all ascribe to PMSMs' various excellent features such as high torque density, high efficiency, high reliability, low maintenance cost, etc. To take advantage of these features, information like rotor position is required in PMSM drive when the field-oriented control (FOC) scheme is adopted [1]-[7]. Usually, a mechanical sensor, such as encoder and resolver, is mounted on the shaft of a PMSM to obtain an accurate rotor position. However, the installation of mechanical sensor not only increases costs but also decreases the reliability of system. Occasionally, there is no enough space to mount a mechanical sensor. Therefore, various kinds of rotor position estimation methods that help to remove mechanical sensor in PMSMs drive systems have been proposed in past decades.

In medium- and high-speed regions, most of the rotor position estimation methods are based on the existence of back electromotive force (EMF), since the back EMF induced by permanent magnet is proportional to the rotor speed which can be seen from the mathematical equation of the PMSM [8], [9]. However, when the PMSM operates in low-speed region and standstill, the back EMF of the PMSM drops to very low amplitude even nil.

To overcome the drawback of deteriorated back EMF in low-speed range, various position estimation methods that are mainly for low-speed PMSMs sensorless control have been proposed. Among them, high frequency signal injection methods play crucial roles [10], [11]. Due to the existence of saliency effect in interior PMSMs (IPMSMs), the winding inductance can be expressed as rotor position concerned equations when the high frequency signal is injected, then the rotor position can be extracted from the equations. In the past decades, researches on high frequency signal injection methods have been progressed considerably. These high frequency injection based methods are exploited from standstill to low speeds, and can be classified into two categories, the continuous and the transient signal injection methods, according to [12]-[14]. For the continuous signal injection methods, a continuous high frequency signal is superimposed onto the fundamental armature voltage commands, which has an amplitude varying from several tens to over one hundred volts. The injected high frequency components can be a sinusoidal signal, a square-wave signal or a pulsating signal. For the transient signal injection methods, the rotor position information is extracted from the transient response of the stator current after an impulse voltage vector is applied [15], [16]. For example, the Indirect Flux Detection by On-line Reactance Measurement (INFORM) is a typical application of transient injection method. However, all of the methods inevitably generate acoustic noise, high torque ripples as well as harmonic losses as results of the injected high frequency components. To suppress acoustic noise, methods like pseudorandom high frequency signal injection and random switching techniques have been proposed in [17], [18]. By injecting a variable high frequency signal, the acoustic noise

Manuscript received June 30, 2017; accepted October 23, 2017. This work was supported by the Research Fund for the National Science Foundation of China (51690182).

The authors are with the School of Electrical Engineering and Automation, Harbin Institute of Technology, Harbin 150001, China (e-mail: WGL818 @hit.edu.cn; junyao.kuang@gmail.com; znn429@126.com; wisdom9527 @163.com; xudiang@hit.edu.cn).

can be reduced to a relatively lower level. Nonetheless, torque ripples and harmonic losses remain unsolved problems.

Therefore, position estimation methods which use the stator current derivatives have been proposed to avoid aforementioned drawbacks [19]-[23]. In these methods, the accuracy of sampled current derivatives is vital in the process of rotor position calculation. In FOC schemes, which are based on the standard vector control principle, the zero voltage vector (ZVV) period can be used to calculate current derivatives. Since a control period is composed of effective vectors and ZVVs. In low-speed range, the zero voltage time increases tremendously due to the low amplitude back EMF. This low-speed attribute enables the obtaining of three phase currents and their derivatives during the zero voltage time. In conventional rotor position estimation methods, current derivatives during the zero voltage period are obtained through a specially designed apparatus, by using Rogowski coil, for example, or by calculating discrete current slope from repeatedly sampled current through an extra high resolution A/D converter during the ZVV time. However, either additional excessive current derivative sensors or high resolution current sensors are not economic and reliable in industrial applications. Therefore, low-speed position estimation methods that use ZVV derivatives were proposed in [21], [23]. In these methods, current derivatives are calculated during ZVV period, and switching rules between light load and heavy load regions are used for achieving the full-load range operation. In [22], a q-axis current based position estimation method that can avoid a switching manipulation is presented. However, high-amplitude d-axis current injection is required from no-load to rated load.

In this paper, a position estimation method that is based on ZVV injection is proposed to achieve low- and zero-speed operation of sensorless IPMSM drives. This investigation mainly focuses on the position information extraction from ZVV period without high-frequency signal injection. And the main contributions of the paper are categorized in three aspects. First, in order to achieve full-load range operation without switching manipulations, a d-axis current allocation scheme is introduced. In addition, a modified SVPWM control scheme and a ZVV extension method, which help to improve the accuracy of calculated current derivatives, are presented in the position estimation process. Further, a novel current sampling scheme that selects two suitable phase currents according to the voltage sector location is adopted to improve the estimation accuracy of rotor position. Experimental results on an IPMSM drive platform validate the effectiveness of the proposed method.

II. Mathematical Analysis of Rotor Position Estimation When Zero Voltage Vector is Applied

A. Modeling of PMSMs for zero voltage injection method

The voltage equation of PMSMs in the d-q synchronous reference frame can be expressed as [24]

$$\begin{bmatrix} u_d \\ u_q \end{bmatrix} = R\begin{bmatrix} i_d \\ i_q \end{bmatrix} + p\begin{bmatrix} \psi_d \\ \psi_q \end{bmatrix} + \omega\begin{bmatrix} -\psi_q \\ \psi_d \end{bmatrix} \tag{1}$$

where u_d, u_q, i_d, i_q, ω and R are the stator voltages, the stator currents, the rotor speed and the stator resistance, respectively, p represents the differential operator, while ψ_d and ψ_q are the flux linkages and can be expressed as

$$\begin{bmatrix} \psi_d \\ \psi_q \end{bmatrix} = \begin{bmatrix} L_d & 0 \\ 0 & L_q \end{bmatrix}\begin{bmatrix} i_d \\ i_q \end{bmatrix} + \begin{bmatrix} \psi_f \\ 0 \end{bmatrix} \tag{2}$$

where L_d, L_q and ψ_f are the d-q synchronous frame inductances and the permanent magnet flux linkage, respectively.

Substituting ψ_d and ψ_q in (1) with (2), yielding

$$\begin{bmatrix} u_d \\ u_q \end{bmatrix} = R\begin{bmatrix} i_d \\ i_q \end{bmatrix} + \begin{bmatrix} pL_d & -L_q\omega \\ L_d\omega & pL_q \end{bmatrix}\begin{bmatrix} i_d \\ i_q \end{bmatrix} + \omega\begin{bmatrix} 0 \\ \psi_f \end{bmatrix}. \tag{3}$$

Transforming (2) from the rotating frame to the stationary frame, the voltage equation can be expressed as

$$\begin{aligned} \begin{bmatrix} u_\alpha \\ u_\beta \end{bmatrix} &= R\begin{bmatrix} i_\alpha \\ i_\beta \end{bmatrix} + \begin{bmatrix} \Sigma L+\Delta L\cos 2\theta_e & \Delta L\sin 2\theta_e \\ \Delta L\sin 2\theta_e & \Sigma L-\Delta L\cos 2\theta_e \end{bmatrix} p\begin{bmatrix} i_\alpha \\ i_\beta \end{bmatrix} \\ &+ \omega\begin{bmatrix} -2\Delta L\sin 2\theta_e & 2\Delta L\sin 2\theta_e \\ 2\Delta L\cos 2\theta_e & 2\Delta L\cos 2\theta_e \end{bmatrix}\begin{bmatrix} i_\alpha \\ i_\beta \end{bmatrix} + \psi_f\omega\begin{bmatrix} -\sin\theta_e \\ \cos\theta_e \end{bmatrix} \end{aligned} \tag{4}$$

where u_α, u_β, i_α, and i_β are the voltages and currents components in the stationary reference frame, θ_e is the electrical rotor position. ΣL and ΔL are the average and difference inductances, and are defined as $\Sigma L = (L_d + L_q)/2$, and $\Delta L = (L_d - L_q)/2$, respectively.

When the ZVV is applied, the superimposed voltage to the PMSM is null, and the PMSM equation is expressed as

$$\begin{aligned} \boldsymbol{Y}_d \cdot p\begin{bmatrix} i_\alpha \\ i_\beta \end{bmatrix} &= -R\begin{bmatrix} i_\alpha \\ i_\beta \end{bmatrix} - \psi_f\omega\begin{bmatrix} -\sin\theta_e \\ \cos\theta_e \end{bmatrix} \\ &- \omega\begin{bmatrix} -2\Delta L\sin 2\theta_e & 2\Delta L\sin 2\theta_e \\ 2\Delta L\cos 2\theta_e & 2\Delta L\cos 2\theta_e \end{bmatrix}\begin{bmatrix} i_\alpha \\ i_\beta \end{bmatrix} \end{aligned} \tag{5}$$

where $\boldsymbol{Y}_d$ represents the inductance matrix and can be expressed as

$$\boldsymbol{Y}_d = \begin{bmatrix} \Sigma L+\Delta L\cos 2\theta_e & \Delta L\sin 2\theta_e \\ \Delta L\sin 2\theta_e & \Sigma L-\Delta L\cos 2\theta_e \end{bmatrix}. \tag{6}$$

In (5), the term in the left is the current derivatives which can be detected or calculated. The first term in the right side is the voltage drop across the stator resistance. In most of the cases, it is regarded as a negligible term since it has a very-low amplitude compared to the rest terms. However, the voltage drop across the stator resistance contributes a fairly large proportion since the other two terms which contain the speed parameter are all small variables when the motor operates in low-speed region especially at standstill. The second term is induced by permanent magnet flux, while the third term exists due to saliency effect.

To simplify (5), by multiplying the inverse matrix of $\boldsymbol{Y}_d$ in both sides, the equation can be expressed as functions of the stationary frame currents i_α and i_β as shown in (7).

Therefore, the PMSM equations in the stationary frame are obtained when the ZVV is applied. From (7), it can be observed that the speed and the position information exists both in the coefficients of the stationary frame current terms and the back EMF terms. The amplitude of the third term in the right dies down with the decrease of the operating speed. Hence, separating the coupled speed and position is necessary in the position estimation process. There are two solutions considered to solve this problem. One is to eliminate the speed in the two

This article has been accepted for publication in a future issue of this journal, but has not been fully edited. Content may change prior to final publication. Citation information: DOI 10.1109/TPEL.2017.2767294, IEEE Transactions on Power Electronics

$$\begin{cases} \dfrac{di_\alpha}{dt} = \dfrac{1}{L_d L_q}\{2\Sigma L\Delta L\omega\sin 2\theta_e - R(\Sigma L - \Delta L\cos 2\theta_e)\cdot i_\alpha \\ \quad -2\Delta L(\Sigma L\omega\cos 2\theta_e - 2\Delta L\omega - R\sin 2\theta_e)\cdot i_\beta\} \\ \quad +\dfrac{\psi_f\omega}{L_q}\sin\theta_e \\ \dfrac{di_\beta}{dt} = \dfrac{1}{L_d L_q}\{2\Delta L(R\sin 2\theta_e - \Sigma L\omega\cos 2\theta_e - 2\Delta L\omega)\cdot i_\alpha \\ \quad -R(\Sigma L + \Delta L\cos 2\theta_e) + 2\Sigma L\Delta L\omega\sin 2\theta_e\cdot i_\beta\} \\ \quad -\dfrac{\psi_f\omega}{L_q}\cos\theta_e \end{cases} \tag{7}$$

equations and calculate the rotor position directly. The other is to eliminate the θ_e by manipulating the two equations in (7), and then calculating the rotor position by integrating the remaining ω. Actually, it is not practical for the first solution since the speed dies down to low amplitude signals and even can be regarded as noises when the operating speed approaches standstill. Thus, an advantageous method eliminating terms pertaining to rotor position will be introduced in the next part.

B. Analysis of rotor position estimation scheme

Fig. 1 shows the proposed sensorless control scheme. In the diagram, the stationary frame currents are used to estimate the rotor position and speed.

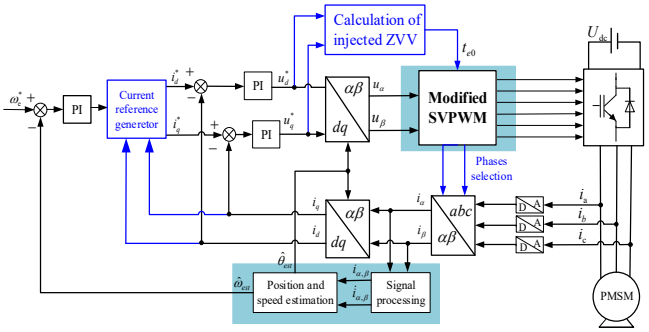

Fig. 1. Proposed sensorless FOC scheme for the PMSM.

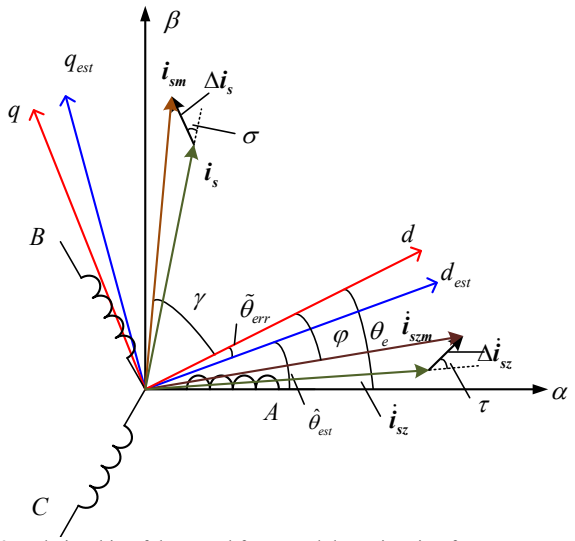

Fig. 2. Relationship of the actual frame and the estimation frame.

Considering an estimated *d*-*q* frame, d_{est}-q_{est} frame, as shown in Fig. 2, the estimated electrical rotor position is $\hat{\theta}_{est}$ and the offset from the real rotor position is [25]

$$\tilde{\theta}_{err} = \theta_e - \hat{\theta}_{est}\,. \tag{8}$$

Actually, the current derivatives in (7) can be regarded as independent variables, since the current derivatives in the stationary frame are calculated from separately sampled current groups during ZVV intervals. To eliminate terms relating to the rotor position in current coefficients, the phase locked loop method is adopted. Multiplying $\sin\hat{\theta}_{est}$ for terms reflected in α-axis, and multiplying $\cos\hat{\theta}_{est}$ for terms reflected in β-axis in (7), the equation can be re-written as (9) and (10).

$$\begin{aligned} \frac{di_\alpha}{dt}\sin\hat{\theta}_{est} = \frac{1}{L_d L_q}\{&2\Sigma L\Delta L\omega\sin 2\theta_e\sin\hat{\theta}_{est}\cdot i_\alpha \\ &-R(\Sigma L\sin\hat{\theta}_{est} - \Delta L\cos 2\theta_e\sin\hat{\theta}_{est})\cdot i_\alpha \\ &-2\Delta L\omega(\Sigma L\cos 2\theta_e - 2\Delta L)\sin\hat{\theta}_{est}\cdot i_\beta \\ &+2R\Delta L\sin 2\theta_e\sin\hat{\theta}_{est}\cdot i_\beta\} \\ &+\frac{\psi_f}{L_q}\omega\sin\theta_e\sin\hat{\theta}_{est} \end{aligned} \tag{9}$$

$$\begin{aligned} \frac{di_\beta}{dt}\cos\hat{\theta}_{est} = \frac{1}{L_d L_q}\{&R\Delta L\sin 2\theta_e\cos\hat{\theta}_{est}\cdot i_\alpha \\ &-2\Delta L\omega(\Sigma L\cos 2\theta_e\cos\hat{\theta}_{est} - \cos\hat{\theta}_{est})\cdot i_\alpha \\ &-2\Sigma L\Delta L\omega\sin 2\theta_e\cos\hat{\theta}_{est}\cdot i_\beta \\ &-R(\Sigma L\cos\hat{\theta}_{est} + \Delta L\cos 2\theta_e\cos\hat{\theta}_{est})\cdot i_\beta\} \\ &-\frac{\psi_f\omega}{L_q}\cos\theta_e\cos\hat{\theta}_{est} \end{aligned} \tag{10}$$

Subtracting (10) from (9), the obtained equation is expressed as

$$\begin{aligned} \frac{di_\alpha}{dt}\sin\hat{\theta}_{est} - \frac{di_\beta}{dt}\cos\hat{\theta}_{est} = &\\ \frac{1}{L_d L_q}\{&2\Delta L\Sigma L\omega\cos(2\theta_e - \hat{\theta}_{est})\cdot i_\alpha \\ &-R(\Sigma L\sin\hat{\theta}_{est} + \Delta L\sin(2\theta_e - \hat{\theta}_{est}))\cdot i_\alpha \\ &+R(\Sigma L\cos\hat{\theta}_{est} + \Delta L\cos(2\theta_e - \hat{\theta}_{est}))\cdot i_\beta \\ &+2\Sigma L\Delta L\omega\sin(2\theta_e - \hat{\theta}_{est})\cdot i_\beta \\ &+2\Delta L^2\omega\cdot(i_\alpha\cos\hat{\theta}_{est} + i_\beta\sin\hat{\theta}_{est})\} \\ &+\frac{\psi_f\omega}{L_q}\cos(\theta_e - \hat{\theta}_{est}) \end{aligned} \tag{11}$$

From (11), it can be seen that the coefficients of stationary frame currents contain the position information. To eliminate $2\theta_e - \hat{\theta}_{est}$ terms, the following can be substituted into (11)

$$2\theta_e - \hat{\theta}_{est} = \hat{\theta}_{est} + 2\tilde{\theta}_{err} \tag{12}$$

When the estimated rotor position approaches the real rotor position, the position error $\tilde{\theta}_{err}$ converges to zero. According to the Taylor expansion, the following approximate equation is valid,

$$\cos(\hat{\theta}_{est}+2\tilde{\theta}_{err})=\cos\hat{\theta}_{est}-\frac{1}{2!}(2\tilde{\theta}_{err})^2+o(\tilde{\theta}_{err}^2)\cong\cos\hat{\theta}_{est}, \quad (13)$$

$$\sin(\hat{\theta}_{est}+2\tilde{\theta}_{err})=\sin\hat{\theta}_{est}+2\tilde{\theta}_{err}+o(\tilde{\theta}_{err})\cong\sin\hat{\theta}_{est}. \quad (14)$$

By substituting (13), (14) into (11), the simplified equation is rewritten as

$$\begin{aligned}L_q\left(\frac{di_\alpha}{dt}\sin\hat{\theta}_{est}-\frac{di_\beta}{dt}\cos\hat{\theta}_{est}\right)=&\\ R(i_\beta\cos\hat{\theta}_{est}-i_\alpha\sin\hat{\theta}_{est})&\\ +2\Delta L(i_\alpha\cos\hat{\theta}_{est}+i_\beta\sin\hat{\theta}_{est})\cdot\omega&\\ +\psi_f\cos\tilde{\theta}_{err}\cdot\omega&\end{aligned} \quad (15)$$

For (15), considering the second term in the right side, when the position estimation method is applied in a surface-mounted PMSM drives, it is clear that it can be neglected since the difference inductance in SPMSM is zero. However, this term is a non-zero quantity in IPMSM drive applications. Actually, the expression $i_\alpha\cos\hat{\theta}_{est}+i_\beta\sin\hat{\theta}_{est}$ can be approximately regarded as the *d*-axis current if the estimated rotor position approaches the actual rotor position. In addition, the second term is a smaller quantity compared with the permanent magnet flux linkage which is shown in the third term, and the two terms both contain rotor speed. For the third term, considering $\cos\tilde{\theta}_{err}\cong1$, this condition is fulfilled in a relatively large scale of $\tilde{\theta}_{err}$, since the Taylor expansion of cosine function converges to unitary in second order in the immediate zero range. The actual speed in the equation can be replaced by the estimated speed when the estimation method converges,

$$\omega\cong\hat{\omega}_{est}=\frac{d\hat{\theta}_{est}}{dt}. \quad (16)$$

Therefore, (15) can be simplified and expressed as

$$\left(\frac{di_\alpha}{dt}+\frac{R}{L_q}i_\alpha\right)\cdot\sin\hat{\theta}_{est}-\left(\frac{di_\beta}{dt}+\frac{R}{L_q}i_\beta\right)\cdot\cos\hat{\theta}_{est}=\frac{\psi_f}{L_q}\frac{d\hat{\theta}_{est}}{dt}. \quad (17)$$

(17) is the PMSM equation in the ZVV period. Different from the conventional motor equation which is based on states of currents and voltages, equation (17) establishes an input-output relationship among the rotor position, the stator currents and the current derivatives. The rotor speed is a non-zero quantity as long as the motor rotates. It means that conventional position observers which are based on current state equations cannot be applied into this control scheme. However, the rotor position can be calculated by integrating the left side,

$$\begin{aligned}\hat{\theta}_{est}^{n+1}=&\hat{\theta}_{est}^{n}\\ &+\frac{L_qT_s}{\psi_f}\left(\frac{di_\alpha}{dt}\sin\hat{\theta}_{est}-\frac{di_\beta}{dt}\cos\hat{\theta}_{est}+\frac{R}{L_q}i_\alpha\sin\hat{\theta}_{est}-\frac{R}{L_q}i_\beta\cos\hat{\theta}_{est}\right)\end{aligned} \quad (18)$$

where T_s is the control period and n is the calculating index representing the time instant $t=nT_s$.

From (18), it can be seen that the electrical rotor position is calculated by integrating terms related to stator currents and current derivatives. As aforementioned, the four variables can be measured or calculated through measured parameters, and all the four variables are multiplied by a term pertaining to $\hat{\theta}_{est}$.

Thus, the rotor position estimation scheme can be realized by a phase locked loop, as shown in Fig. 3.

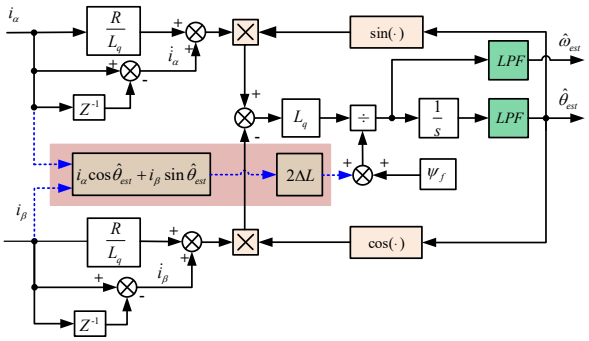

Fig. 3. Proposed position estimation scheme.

In Fig. 3, the dash line shows the term relating to the difference inductance. It can be neglected in the surface-mounted SPMSM drive application, since the inductance difference in SPMSMs is zero. However, it should be taken into consideration when applying in the IPMSM drives if the IPMSM has a large inductance difference. From (18) and the control scheme in Fig. 3, it can be seen that the implementation of the proposed position estimation method necessitates maintaining the coefficients of $\sin\hat{\theta}_{est}$ and $\cos\hat{\theta}_{est}$ non-constant zero value. In medium- and heavy-load regions, the requirements are unconditionally satisfied as the existence of high-amplitude *q*-axis current. In no-load and light-load regions, to ensure the proposed method can be employed successfully, the *d*-axis current should be regulated to a non-zero value by modifying the reference of i_d as shown in Fig.1.

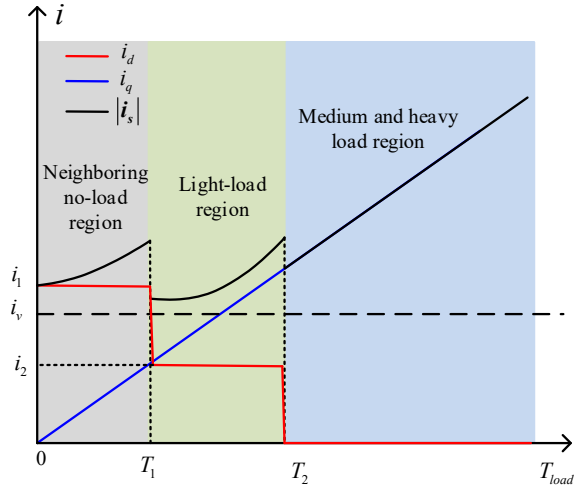

Fig. 4. Arrangement of *dq* frame current according to load torque.

The current allocation scheme is shown in Fig. 4. $\boldsymbol{i_s}$ is the stator current vector which is synthesized by i_d and i_q. i_v is the minimum value that enables the method smoothing. In nearing no-load region, i.e. load torque lower than T_1 shown in Fig. 4, a high amplitude current i_1 is injected to *d*-axis. In light-load region, i.e. load torque between T_1 and T_2, the given current of i_d is set to a lower amplitude i_2 for the sake of power loss reduction. In medium- and heavy-load region, i_d is set to zero.

This article has been accepted for publication in a future issue of this journal, but has not been fully edited. Content may change prior to final publication. Citation information: DOI 10.1109/TPEL.2017.2767294, IEEE Transactions on Power Electronics

Hence, the amplitude of synthesized vector $\boldsymbol{i}_s$ can be maintained to larger than i_v from no-load to rated load.

As discussed before, in neighboring no-load region, if the *d*-axis current is set to a large value in an IPMSM drive system, it should be taken into calculation to compensate the error caused by the injected *d*-axis current, as the dash line loop shown in Fig. 3. In addition, the inverter switching period is small with respect to the electrical time constant of the motor [23]. It is possible to use the *d*-axis current reference i_d^* to the estimation loop instead of calculating $i_\alpha \cos\hat{\theta}_{est} + i_\beta \sin\hat{\theta}_{est}$.

In IPMSM control, the influence of armature-reaction magnetic field on saturation can be neglected when the stator current is very small. However, when IPMSMs operate in heavy-load region, the armature-reaction will affect the *dq* frame inductances [26]. The *q*-axis inductance is shown in the proposed position estimation process, thus the variation of *q*-axis inductance should be restricted to a certain extent to enable the application of the proposed method. However, there is no need to take the *d*-axis inductance variation into account, since the *d*-axis inductance is absent in the position estimation equation.

III. Current Sampling Method for Derivative Error Reduction

From (18), it can be seen that the accuracy of sampled currents and current derivatives will decide the level of position error of the proposed method. There are some papers already presented current derivatives detection or calculation methods, but are all based on special designed current differential detectors or extra high resolution current sensors, which all inevitably increase system complexity and expenses [18], [19]. In order to make this technique more suitable for industrial applications, a simple but reliable current sampling method is introduced in this section, as well as an improved current derivative calculation scheme.

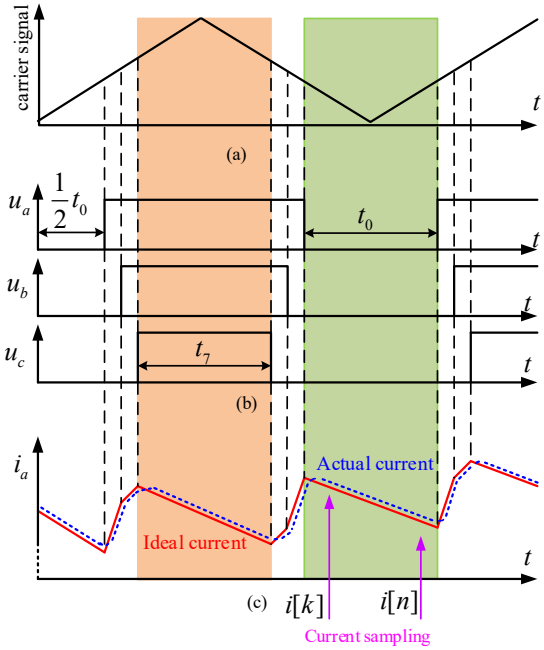

Fig. 5. Traditional current sampling method. (a) Carrier wave of FOC scheme. (b) Three phase switching signals. (c) comparison of ideal and actual phase current wave.

The traditional current sampling method is shown in Fig.5. In each control period, the generated effective vector to offset back EMF is relatively small in low-speed region and standstill. However, this effect brings about benefits to this control scheme, e.g., long ZVV period, as shown in Fig. 5 (b). The current diagram in Fig. 5 (c) shows the periodic fluctuation of one phase current during one control period. The polyline is the expected current curve, while the dash line shows the real current to be sampled. As it can be observed, since the existence of low pass filtering effect between the shunt resistance and the A/D converter, there is always an error between the real current and the expected current curve [27]. Therefore, the current should be sampled after a short time delay when the zero voltage interval starts. Actually, other factors such as the dead time and IGBT turn-on and -off should also be taken into account. It is known that during the turn-off period, the IGBT current will decrease gradually, which will affect the accuracy of sampled current significantly. The solution to this problem will be discussed later.

As analyzed in section II, the rotor position information is extracted from the transient state of the closed loop control scheme. The calculation process is fed by the sampled currents, which are normally affected by noise, distortion, resolution of A/D converter as well as nonlinearity during the sampling procedure [28], [29]. Additionally, when calculating current derivatives, it will inevitably involve the division of time difference of sampled currents. Consequently, truncation error is introduced to current derivatives. Considering re-written (17) by substituting stationary frame currents with the synthesized rotational vector $\boldsymbol{i}_s$ and substituting current derivatives with synthesized rotational vector $\dot{\boldsymbol{i}}_{sz}$ which can be expressed as

$$i_\alpha = |\boldsymbol{i}_s|\cos(\gamma+\theta_e),\ i_\beta = |\boldsymbol{i}_s|\sin(\gamma+\theta_e) \tag{19}$$

and

$$\dot{i}_\alpha = |\dot{\boldsymbol{i}}_{sz}|\cos(-\varphi+\theta_e),\ \dot{i}_\beta = |\dot{\boldsymbol{i}}_{sz}|\sin(-\varphi+\theta_e) \tag{20}$$

where γ represents angle gap between the current vector and the *d*-axis, φ is the angle gap between the current derivative vector and the *d*-axis, respectively, as shown in Fig. 2.

Substituting (19) and (20) into (17), the following result can be obtained

$$-\frac{1}{\psi_f}(L_q|\dot{\boldsymbol{i}}_{sz}|\sin(\tilde{\theta}_{err}-\varphi)+R|\boldsymbol{i}_s|\sin(\tilde{\theta}_{err}+\gamma)) = \hat{\omega}_{est}. \tag{21}$$

Suppose the sampling errors are both experienced in the currents and the current derivatives [17]:

$$\dot{\boldsymbol{i}}_{szm} = \dot{\boldsymbol{i}}_{sz} + \Delta\dot{\boldsymbol{i}}_{sz} \text{ and } \boldsymbol{i}_{sm} = \boldsymbol{i}_s + \Delta\boldsymbol{i}_s \tag{22}$$

where $\boldsymbol{i}_{sm}$, $\dot{\boldsymbol{i}}_{szm}$, $\Delta\boldsymbol{i}_s$ and $\Delta\dot{\boldsymbol{i}}_{sz}$ are the sampling current vector, the current derivative vector, the sampling current error vector and the current derivative error vector, respectively. The angle between $\Delta\boldsymbol{i}_s$ and $\boldsymbol{i}_s$ is σ, and the angle between $\Delta\dot{\boldsymbol{i}}_{sz}$ and $\dot{\boldsymbol{i}}_{szm}$ is τ, as shown in Fig. 2.

The rotor position error caused by errors of currents and current derivatives is calculated as follow

$$\begin{aligned}\theta_e - \hat{\theta}_{est} &= \Delta\hat{\omega}_{est}T_s \\ &= \frac{T_s}{\psi_f}(L_q|\Delta\dot{\boldsymbol{i}}_{sz}|\sin(\tilde{\theta}_{err}-\varphi+\tau)+R|\Delta\boldsymbol{i}_s|\sin(\tilde{\theta}_{err}+\gamma+\sigma))\end{aligned} \tag{23}$$

This article has been accepted for publication in a future issue of this journal, but has not been fully edited. Content may change prior to final publication. Citation information: DOI 10.1109/TPEL.2017.2767294, IEEE Transactions on Power Electronics

where $\Delta\hat{\omega}_{est}$ is the speed error.

In (17) and (23), the speed estimation process can be regarded as a zero input resistor-inductor circuit during the zero voltage period. The noise of current will definitely affect the results of estimated rotor speed and position. Moreover, the position error caused by truncation error of calculated current derivatives should also be taken into account. In fact, the electrical time constant L_q/R is a much smaller quantity in comparison with the mechanical time constant [30]. This characteristic ensures that the real speed is maintained constant though there always exist torque ripples during short-term operation. So, a filtering action is needed in the estimation loop to obtain a smooth estimate speed. In addition, the dynamic of the velocity loop is slower than the current loop as well known. Hence, two different order low pass filters are applied to filter the speed and position information respectively. Consequently, a phase lag will be introduced to the control loop. Further, the low pass filtering effect between the current shunt resistor and the A/D converter in the sampling circuit also provides the phase lag. However, when there is a small error in measurement and parameters, these effects will be decreased greatly. Improving the accuracy of sampled currents and current derivatives can help solve the problems.

Generally, in order to reduce switching loss and high frequency components, the entire zero voltage time is divided into two equal parts, t_0 and t_7, in conventional control scheme, as shown in Fig. 5 (b). Fig. 6 shows the proposed modified SVPWM method for acquiring the rotor position more effectively. To take advantage of the relatively shorter period of the effective vector, the proportion of zero voltage intervals t_0 and t_7 is tuned, as shown in Fig. 6. In addition, a ZVV is inserted between each carrier signal according to load torque and rotor speed as shown in Fig. 1. Occasionally, torque disturbance or speed variation may cause the increase of effective vectors, and as a consequence, t_0 is not enough to calculate current derivatives. Hence, the injecting of ZVV is necessary. However, the injected ZVV will not limit the bandwidth significantly since the control period has not been extended too much. The time difference Δt between two sampled current groups can be set to a desired value by modifying the length of t_{e0} for the convenience of current derivative calculation and for the sake of truncation error reduction.

Current sampling methods during ZVV time are analyzed in Fig. 6. A method that samples the currents for several consecutive times in each start and end of zero voltage vector intervals is utilized to calculate the current slope instead of a two-point method. Apparently, it can help reduce the disturbance and errors caused by hardware circuits, and the results are verified by experimental results in Part IV.

The current derivative calculation formula is described as

$$\dot{i}_{sp} = \frac{\sum_{k=m+1}^{2m} i_{sp}[k] - \sum_{n=1}^{m} i_{sp}[n]}{m\Delta t} \tag{24}$$

where the subscript sp denotes a, b, c. Δt represents sampling time difference, m is the sampling times in the start and end of each zero voltage interval.

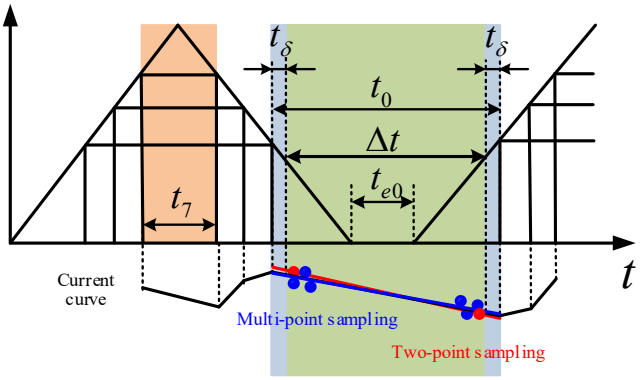

Fig. 6. Zero voltage period extension scheme and current sampling methods.

To reduce the dead time effect and the current ripples aroused by IGBT turn-on and -off, a modified current sampling method is used as shown in Fig. 7. As it is known, the conclusion that the sum of three phase currents is zero is valid at any moment. Therefore, stationary frame current derivatives can be calculated by two of the three phase currents. For example, in sector I and sector VI of six FOC sectors shown in Fig. 7, i_b and i_c will be used to calculate current derivatives, since in sector I and sector VI, the zero voltage interval t_0 begins with the switching off of phase A as shown in Fig. 5(b). Phase B and phase C switch off earlier than phase A as the existence of effective vectors, the dead time effect and current ripple caused by IGBT turn-off will be drastically reduced if calculating current derivatives by using phase B and phase C.

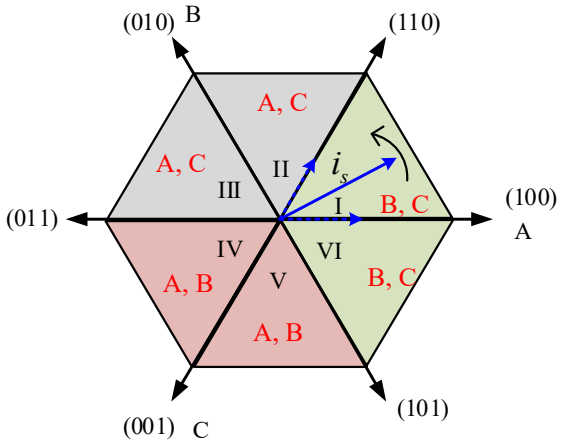

Fig. 7. Relationship of current vector location and corresponding current sampling selection.

IV. Experimental Results

The ZVV injection based sensorless control scheme is verified on a 1.0-kW IPMSM, supplied by a voltage source inverter as shown in Fig. 8. The parameters of IPMSM are shown in Table I. A mechanically coupled load IPMSM is employed to produce the load torque. The sensorless control algorithm system is implemented through a low-cost ARM chip STM32F103VCT6. The unmodified PWM switching frequency of the inverter is 6 kHz. The current sampling procedure is completed through a built-in 12 bits A/D converter, and the current sampling range is restricted to -12.5A to +12.5A, in order to balance an accessible current sampling resolution.

This article has been accepted for publication in a future issue of this journal, but has not been fully edited. Content may change prior to final publication. Citation information: DOI 10.1109/TPEL.2017.2767294, IEEE Transactions on Power Electronics

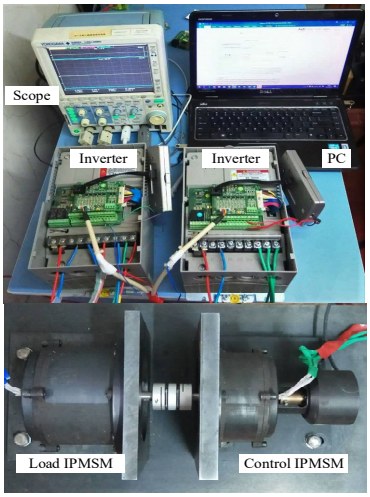

Fig. 8. Experimental test setup of IPMSM drive.

TABLE I
IPMSM PARAMETERS

Parameter	Value	Parameter	Value
Rated Power	1.0kW	Rated Speed	3000r/min
d-axis Inductance	7.9mH	Pole Pairs	3
q-axis Inductance	11.7mH	Resistance	0.74Ω
Torque Constant	0.51N·m/Arms	Flux Linkage	0.374Wb

The comparisons of current response and the corresponding FFT when the proposed ZVV injection method is applied are shown in Fig. 9. By modifying the injected ZVV, the zero voltage period t_0 can be maintained to desired values, i.e. 130us in this experiment. For the aim of balancing an acceptable bandwidth, the entire control period is maintained to no more than 200us. From the results, it can be seen that the modified control scheme has limited influence on the augmentation of current harmonics, and the ZVV period has better current slope response compared to the unmodified method.

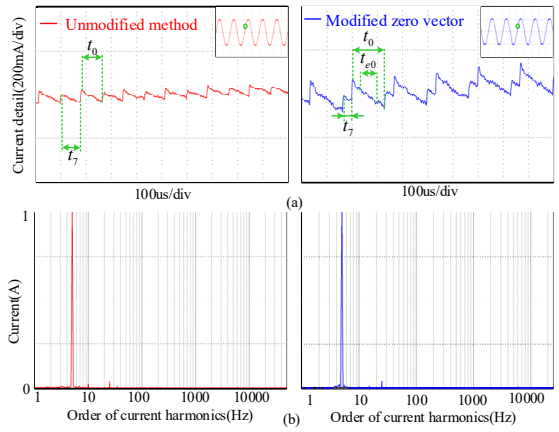

Fig. 9. Comparison of harmonics and current when the proposed ZVV injection method is applied. (a) Stator current waveforms under 100r/min condition. (b) Current harmonic analysis results.

The proposed control strategy based on the proposed two-phase-multi-point current sampling method, multi-point current sampling method and two-point current sampling method are implemented in Fig. 10. The current slopes calculated by the three methods are presented in different colors in the first row of Fig. 10. The reference speed is set as 100r/min under no-load condition, and the *d*-axis current is set to 1.4A. The corresponding estimated rotor electrical position and the position error compared to the real position provided by an incremental encoder are presented in the second row. The diagrams in the third tier show the position error when 43% rated load and full-load torques are imposed. From the results, it can be seen that the proposed two-phase-multi-point sampling method can reduce the calculated current slope noises effectively compared with the other two methods, and the corresponding estimated rotor position matches better the real position, and the positon error is within 10 degrees. In loading conditions, the position error estimated by the two-phase-multi-point current sampling method is within 15 degrees.

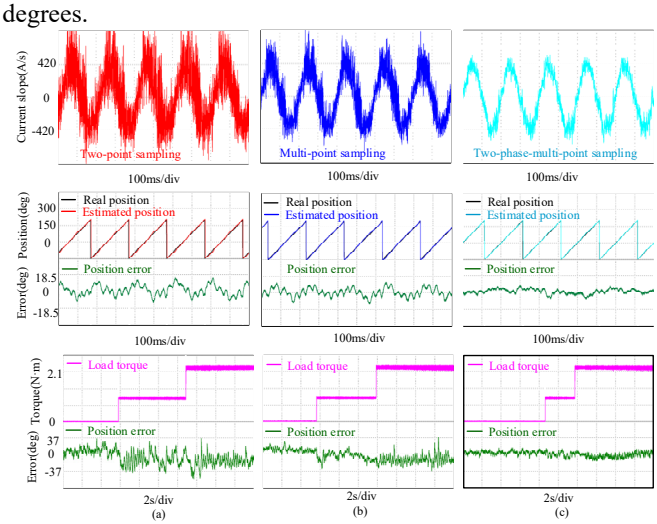

Fig. 10. Experimental comparison of zero voltage period current slopes and estimated position when different current sampling methods are applied under 100r/min and no-load condition. (a) Two-point current sampling method. (b) Multi-point current sampling method. (c) Two-phase-multi-point current sampling method.

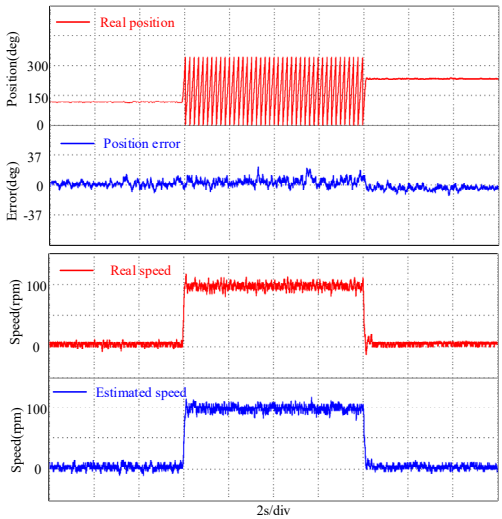

Fig. 11. Dynamic performance under step speed between 0r/min and 100r/min.

Fig. 11 shows the dynamic performance of the proposed position estimation method. The IPMSM subjects to a step speed change from standstill to 100r/min under no-load condition, then the speed goes back to zero. The actual position, the position error and the speed waveforms are shown, respectively. From the results, it can be seen that the position

This article has been accepted for publication in a future issue of this journal, but has not been fully edited. Content may change prior to final publication. Citation information: DOI 10.1109/TPEL.2017.2767294, IEEE Transactions on Power Electronics

error using the two-phase-multi-point sampling method is within 15 degrees during the whole process.

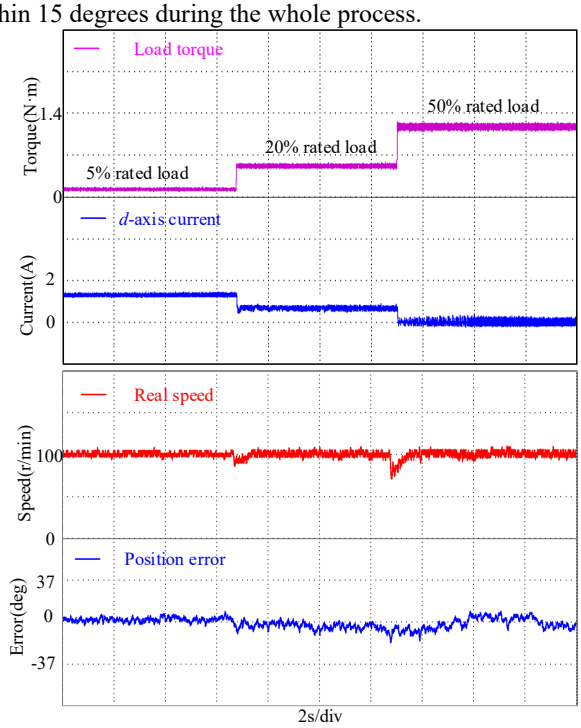

Fig. 12. Allocation of *d*-axis current with respect to variation of load torque.

The amplitude of current vector should always keep above a certain value in order to maintain the successful implementation of the proposed method as mentioned before. In experiments, the i_v is set as 1A. The *d*-axis current is set to 1.4A when the load torque lower 15% rated load. If the IPMSM operates between 15% and 25% rated load, *d*-axis current is set to 0.7A. Otherwise, the *d*-axis current is set to zero. Fig. 12 shows the corresponding experiment of *dq*-axis currents allocation in the three regions. In the experiment, the operating speed is 100r/min, the load given is 5%, 20% and 50% rated load. As can be seen, the position error is within 10 degrees.

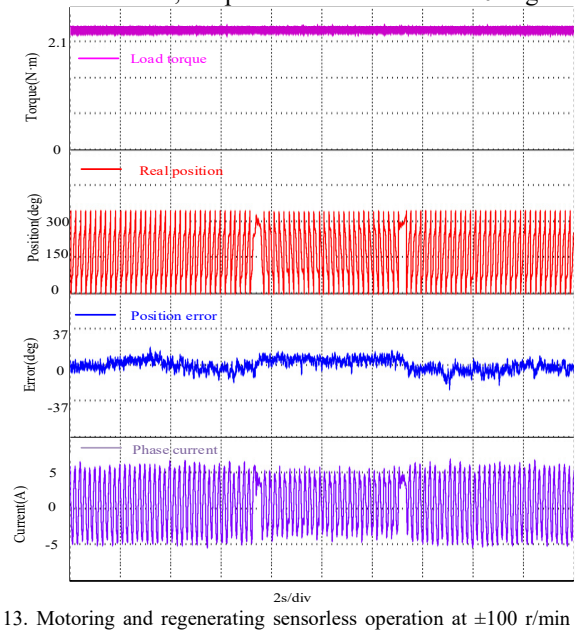

Fig. 13. Motoring and regenerating sensorless operation at ±100 r/min with rated load.

Fig. 13 shows the experimental results of reversal operation under rated load condition. The operating speed of the IPMSM is ±100 r/min. The load torque, the actual rotor position, the estimation errors and the phase current are shown, respectively. From the results, it can be observed that the proposed position estimation method can operate both in motoring and regenerating mode. The position estimation error is within 15 degrees during the whole process.

The experimental results of zero speed with rated step load disturbance sensorless control of IPMSM are shown in Fig. 14. As can be seen, the speed and position error fluctuate at the moments when step load is imposed and removed. In steady state, both speed and position error regress to a normal level. The position error is within 20 degrees during the entire process. Besides, the experimental results also demonstrate that the proposed position estimation method has a good robustness performance in step load condition.

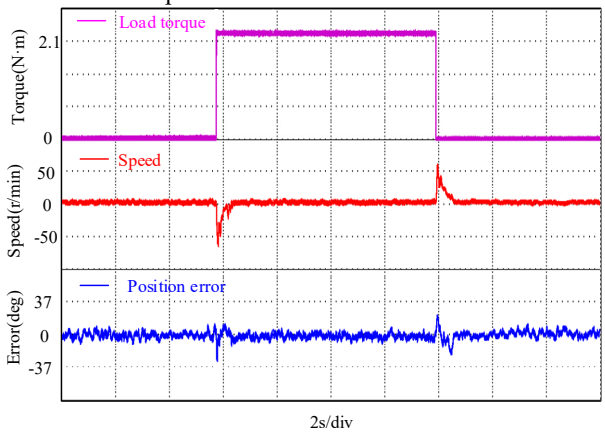

Fig. 14. Sensorless operation at zero speed with rated load disturbance.

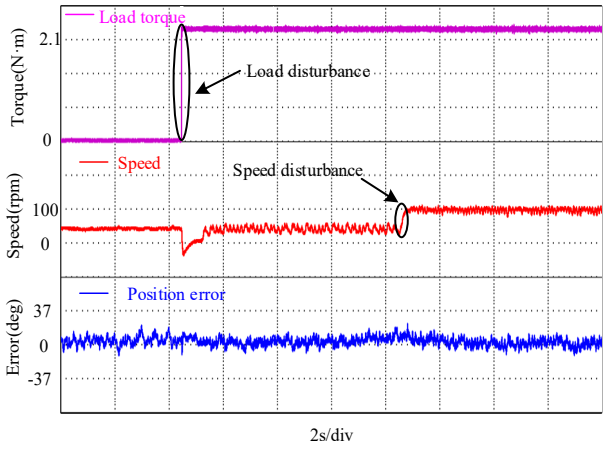

Fig. 15. Dynamic performance with load disturbance and speed disturbance, the load disturbance is from no load to rated load under 40r/min and the speed disturbance is from 40r/min to 100r/min.

Fig. 15 shows the dynamic performances with step load disturbance and step speed disturbance. In the experiments, the speed is 40r/min when the rated step load disturbance is imposed. The load torque is then maintained to rated load, the speed reference changes from 40r/min to 100r/min. As can be seen, the maximum position error is within 20 degrees during the whole process.

This article has been accepted for publication in a future issue of this journal, but has not been fully edited. Content may change prior to final publication. Citation information: DOI 10.1109/TPEL.2017.2767294, IEEE Transactions on Power Electronics

The comparison of q-axis current with the proposed method and with encoder is shown in Fig. 16. The load imposed on the shaft from no-load to 35% rated load, then to 67% rated load, and to rated-load. As well known, the electromagnetic torque can be calculated from dq frame currents. In no-load condition, the difference of q-axis current between the proposed method and with encoder reaches its maximum value, which is probably because of the injected high-amplitude d-axis current. However, with the increase of imposed load torque, the q-axis current difference between the two experiments decreases and reaches nearing zero at rated load.

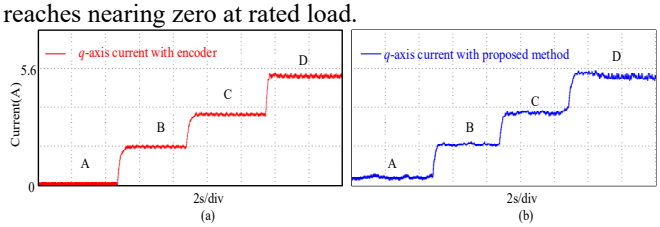

Fig. 16. q-axis current under rated load. (a) q-axis current with encoder. (b) q-axis current with proposed method.

It is difficult to evaluate the effects of inductance variations due to the iron saturation, because when the IPMSM operates in medium or heavy load region, the IPMSM has already experienced an inductance variation. In experiments, there is no online parameter identification method is used to modify the parameters in real time. On this basis, considering changing the q-axis inductance L_q when the IPMSM operates in rated load condition, the experimental results are shown in Fig. 17. As can be seen that the position error is within 10 degrees when the motor suffering a $\pm 6\%$ q-axis inductance variation, and the position error is within 20 degrees when the variation of the q-axis inductance is $\pm 10\%$.

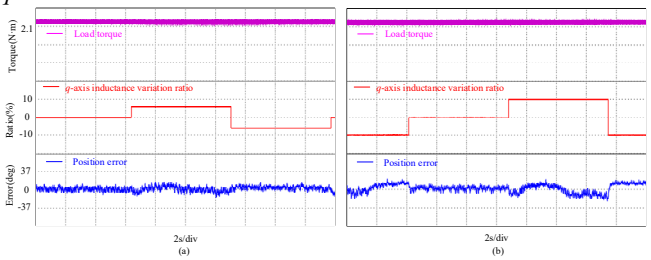

Fig. 17. Position estimation results with inductance variation at rated load. (a) 5% q-axis inductance variation. (b) 10% q-axis inductance variation

V. Conclusion

This paper has proposed a zero voltage vector injection based IPMSM sensorless control scheme, which can reduce the acoustic noises and torque ripples generated by the injected high-frequency signal when the PMSM operates in low-speed range. The rotor position information can be extracted effectively from the current derivatives which are calculated during the zero voltage period, and the injected ZVV does not restrict the instantaneous speed and torque response. The proposed modified SVPWM and current sampling methods can help improve the accuracy of calculated current derivatives and the estimated position. The benefits of the proposed position estimation method are that only simple current shunt resistors is required, and the d-axis current injection is not necessary in heavy-load region, and the estimation scheme is easy to implement. Both the steady and dynamic performances of the proposed sensorless control scheme at low and zero speed operations are verified on a 1.0-kW IPMSM platform.

References

[1] Nahid-Mobarakeh, Babak, F. Meibody-Tabar, and F. M. Sargos. “Back EMF Estimation-Based Sensorless Control of PMSM: Robustness With Respect to Measurement Errors and Inverter Irregularities.” *IEEE Trans. Ind. Electron*., vol. 43, No.2, pp. 485-494, Mar/Apr. 2007.

[2] J. Lemmens, P. Vanassche, and J. Driesen, “PMSM Drive Current and Voltage Limiting as a Constraint Optimal Control Problem.” *IEEE J. Emerg. Sel. Topics Power Electron*., vol. 3, no. 2, p. 326-338, Jun. 2015.

[3] X. Zhang, B. Hou, and M. Yang. “Deadbeat Predictive Current Control of Permanent Magnet Synchronous Motors with Stator Current and Disturbance Observer”, *IEEE Trans. Power Electron.*, vol. 32, no. 5, pp. 3818-3834, May 2017.

[4] Y. Park and S. K. Sul, “Sensorless Control Method for PMSM Based on Frequency-Adaptive Disturbance Observer.” *IEEE J. Emerg. Sel. Topics Power Electron*., vol. 2, pp. 143-151, Jun. 2014.

[5] G. Xie, K. Lu, S. K. Dwivedi, J. R. Rosholm, and F. Blaabjerg. “Minimum-Voltage Vector Injection Method for Sensorless Control of PMSM for Low-Speed Operations.” *IEEE Trans. Power Electron*., vol. 31, no. 2, pp. 1785-1794, Feb. 2016.

[6] G. Zhang, G. Wang, D. Xu, and N. Zhao. "ADALINE-Network-Based PLL for Position Sensorless Interior Permanent Magnet Synchronous Motor Drives", IEEE Trans. Power Electron., vol. 31, no. 2, pp. 1450-1460, Feb. 2016.

[7] P. Dirk, J. F. Stumper, and R. Kennel. “Sensorless Control of Synchronous Machines Based on Direct Speed and Position Estimation in Polar Stator-Current Coordinates.” *IEEE Trans. Power Electron*., vol. 28, no.5, pp. 2503-2513, May. 2013.

[8] S. Zaim, B. Nahid-Mobarakeh, and F. Meibody-Tabar. “Robust Position Sensorless Control of Nonsalient PMSM at Standstill and Low Speeds.” *IEEE J. Emerg. Sel. Topics Power Electron*., vol. 2, no. 3, pp. 640–650, Sept. 2014.

[9] G. Wang, H. Zhan, G. Zhang, X. Gui, and D. Xu. “Adaptive Compensation Method of Position Estimation Harmonic Error for EMF-Based Observer in Sensorless IPMSM Drives.” *IEEE Trans. Power Electron*., vol. 29, no. 6, pp. 3055–3064, Jun. 2014.

[10] R. Ni, D. Xu, F. Blaabjerg, K. Lu, G. Wang, and G. Zhang. “Square-Wave Voltage Injection Algorithm for PMSM Position Sensorless Control With High Robustness to Voltage Errors.” *IEEE Trans. Power Electron*., vol. 32, no. 7, pp. 5425-5437, Sept. 2017.

[11] P. L. Xu, and Z. Q. Zhu. “Novel Square-Wave Signal Injection Method Using Zero-Sequence Voltage for Sensorless Control of PMSM Drives.” *IEEE Trans. Ind. Electron*., vol. 63, no. 12, pp. 7444-7454, Jul. 2016.

[12] D. Raca, P. Garcia, D. O. Reigosa, F. Briz, and R. D. Lorenz. “Carrier Signal Selection for Sensorless Control of PM Synchronous Machines at Zero and Very Low speeds.” *IEEE Trans. Ind. App*, vol. 46, no. 1, pp. 167-178, 2010.

[13] A. R. Setty, S. Wekhande, and K. Chatterjee. “Comparison of High Frequency Signal Injection Techniques for Rotor Position Estimation at Low Speed to Standstill of PMSM.” *IEEE IICPE'2012*, pp.1-6, Dec. 2012.

[14] J. H. Jang, J. I. Ha, M. Ohto, K. Ide, and S. K. SuI. “Analysis of Permanent-Magnet Machine for Sensorless Control Based on High Frequency Signal Injection.” *IEEE Trans. Ind. App*, vol. 40, pp. 1595-1604, Nov./Dec., 2004.

[15] E. Robeischl, and M. Schroedl. “Optimized INFORM-Measurement Sequence for Sensorless PM Synchronous Motor Drives with Respect to Minimum Current Distortion.” *Conf. Rec. IEEE-IAS Annual Meeting*, pp. 92-98, 2002.

[16] Q. Tang, A. Shen, X. Luo, and J. Xu. “PMSM Sensorless Control by Injecting HF Pulsating Carrier Signal Into ABC Frame.” *IEEE Trans. Power Electron*., vol. 32, no. 5, pp. 3767-3776, Jun. 2016.

[17] J. Y. Chai, Y. H. Ho, Y. C. Chang, and C. M. Liaw, “On Acoustic-Noise Reduction Control Using Random Switching Technique for Switch-Mode Rectifiers in PMSM Drive.” *IEEE Trans. Ind. Electron*., vol. 55, no. 3, pp. 1295–1309, Mar. 2008.

[18] G. Wang, L. Yang, G. Zhang, X. Zhang, and D. Xu, “Comparative Investigation of Pseudorandom High-Frequency Signal Injection Schemes for Sensorless IPMSM Drives.” *IEEE Trans. Power Electron.*, vol. 32, no. 3, pp. 2123–2132, March. 2017.

[19] D. Q. Guan, M. X. Bui, D. Xiao, and M. F. Rahman. "Evaluation of an FPGA Current Derivative Measurement System for the Fundamental PWM Excitation Sensorless Method for IPMSM." *IEEE SPEC*'2016, pp. 1-6, Dec. 2016.

[20] Y. Shibano and H. Kubota, "Pole Position Estimation Method of IPMSM at Low Speed without High Frequency Components Injection." *2009 Applied Power Electronics Conference and Exposition,* pp. 233-239, 2009.

[21] Y. Hosogaya and H. Kubota, "Position Estimating Method of IPMSM at Low Speed Region Using dq-axis Current Derivative without High Frequency Component." *IEEE PEDS*'2013, pp.1306-1311, 2013.

[22] Y. Hosogaya and H. Kubota. "Sensorless Control Method of IPMSM with Current Derivative Information of q-axis without High Frequency Component Injection at Low Speed Region." *IEEE ECCE Asia Downunder*, pp. 799-803, Jun. 2013.

[23] Y. Hosogaya and H. Kubota, "Flux Position Estimation Method of IPMSM by Controlling Current Derivative at Zero Voltage Vector." *2010 International Conference on Electrical Machines and Systems,* pp. 894-899, 2012.

[24] X. Luo, Q. Tang, A. Shen, and Q. Zhang, "PMSM sensorless control by injecting HF pulsating carrier signal into estimated fixed-frequency rotating reference frame." *IEEE Trans. Ind. Electron*., vol. 63, no. 4, pp. 2294–2303, Apr. 2016.

[25] A. Mohamed, C. Hackl, and R. Kennel. "Finite Position Set-Phase Locked Loop for Sensorless Control of Direct-Driven Permanent-Magnet Synchronous Generators." *IEEE Trans. Power Electron*., vol. PP, no. 99, pp. 1-1, May. 2017.

[26] X. Chen, J. Wang, B. Sen, P. Lazari, and T. Sun, "A high-fidelity and computationally efficient model for interior permanent-magnet machines considering the magnetic saturation, spatial harmonics, and iron loss effect." *IEEE Trans. Ind. Electron*., vol. 62, no. 7, pp: 4044-4055, July. 2015.

[27] L. Chen and F. Z. Peng, "Dead-time elimination for voltage source inverters." *IEEE Trans. Power Electron*., vol. 23, no. 2, pp. 574–580, Mar. 2008.

[28] S. Bolognani, S. Calligaro and R. Petrella, "Design Issues and Estimation Errors Analysis of Back EMF-Based Position and Speed Observer for SPM Synchronous Motors." *IEEE J. Emerg. Sel. Topics Power Electron*., vol. 2, no.2, pp. 159–170, Jun. 2014.

[29] M. Hinkkanen, T. Tuovinen, L. Harnefors, and J. Luomi, "A Combined Position and Stator-Resistance Observer for Salient PMSM Drives: Design and Stability Analysis." *IEEE Trans. Power Electron*., vol. 27, no. 2, pp. 601–609, 2012.

[30] J. X. Xu, S. K. Panda, Y. J. Pan, T. H. Lee, and B. H. Lam, "A Modular Control Scheme for PMSM Speed Control with Pulsating Torque Minimization." *IEEE Trans. Ind. Electron*., vol. 51, no. 3, pp. 526–536, Jun. 2004.

Gaolin Wang (M'13) received the B.S., M.S. and Ph.D. degrees in Electrical Engineering from Harbin Institute of Technology, Harbin, China, in 2002, 2004 and 2008 respectively.

In 2009, he joined the Department of Electrical Engineering, Harbin Institute of Technology as a Lecturer, where he has been a Full Professor of Electrical Engineering since 2014. From 2009 to 2012, he was a Postdoctoral Fellow in Shanghai Step Electric Corporation, where he was involved in the traction machine control for direct-drive elevators. He has authored more than 60 technical papers published in journals and conference proceedings. He is the holder of 10 Chinese patents. His current major research interests include permanent magnet synchronous motor drives, high performance direct-drive for traction system, position sensorless control of AC motors, efficiency optimization control of PMSM, and digital control of power converters.

Dr. Wang serves as an Associate Editor of IET Electric Power Applications, and Journal of Power Electronics. He received the Outstanding Research Award and the Delta Young Scholar Award from the Delta Environmental and Educational Foundation in 2012 and 2014, respectively. He is currently supported by the National Natural Science of China for Excellent Young Scholars, the Program for Basic Research Excellent Talents and the Young Talent Program from Harbin Institute of Technology.

Junyao Kuang received the B.S. degree in electrical engineering and automation in 2016 from Harbin Institute of Technology, Harbin, China, where he is currently working toward the Master's degree in power electronics and electrical drives with the School of Electrical Engineering and Automation. His current research interests include permanent magnet synchronous motor drives and position sensorless control.

Nannan Zhao received the B.S. and M.S. degrees in control science and engineering from Harbin Institute of Technology, Harbin, China, in 2013 and 2015, respectively, where he is currently working toward Ph.D. degree in power electronics and electrical drives at the School of Electrical Engineering and Automation.

His current research interests include advanced control of permanent magnet synchronous motor drives and position sensor-less control of ac motors.

Guoqiang Zhang received the B.S. degree in Electrical Engineering from Harbin Engineering University, Harbin, China, in 2011, and the M.S. and Ph.D. degrees in Electrical Engineering from Harbin Institute of Technology, Harbin, China, in 2013 and 2017, respectively.

Since then, he has been a Postdoctoral Fellow and a Lecturer in the Department of Electrical Engineering, Harbin Institute of Technology. His current research interests include parameter identification technique, and control of electrical drives, with main focus on sensorless field-oriented control of interior permanent magnet synchronous machines.

Dianguo Xu (M'97, SM'12, Fellow' 17) received the B.S. degree in Control Engineering from Harbin Engineering University, Harbin, China, in 1982, and the M.S. and Ph.D. degrees in Electrical Engineering from Harbin Institute of Technology (HIT), Harbin, China, in 1984 and 1989 respectively.

In 1984, he joined the Department of Electrical Engineering, HIT as an Assistant Professor. Since 1994, he has been a Professor in the Department of Electrical Engineering, HIT. He was the Dean of School of Electrical Engineering and Automation, HIT from 2000 to 2010, and was the Assistant President of HIT from 2010 to 2014. He is now the Vice President of HIT. His research interests include renewable energy generation technology, power quality mitigation, sensorless vector controlled motor drives, high performance PMSM servo system. He published over 600 technical papers.

Dr. Xu is a Fellow of IEEE, an Associate Editor of the IEEE Transactions on Industrial Electronics, and IEEE Journal of Emerging and Selected Topics in Power Electronics. He serves as Chairman of IEEE Harbin Section.